(IJIEST) 2015, Vol. No. 1, Jan-Dec **e-ISSN: 2454-9584; p-ISSN: 2454-8111**

THE EFFECT OF THERMAL ANNEALING ON DEVICE MORPHOLOGY

Dr. Dileep. P.
Lecturer in Electronics
Govt. Polytechnic College, Perinthalmanna, Kerala

ABSTRACT

The bulk heterojunction (BHJ) polymer photovoltaic (PV) cells using a composite of (P3HT) and (PCBM) shows a better performance among the Organic Solar Cells and this has been the most studied and successful system [4,5]. The device morphology has been shown to be a critical parameter governing charge transport properties of polymer bulk heterojunction (BHJ) solar cells. In this AFAM, Atomic Force Spectroscopy and Nanoindentation were used to study the effect of the fullerene presence and the annealing on the P3HT:PCBM nanomechanical behavior. The P3HT:PCBM thin films were prepared by spin coating on glass substrates and then annealed at 100 °C and 145 °C for 30 min. Large phase separation was identified by optical and Atomic Force Microscopy (AFM) for the annealed samples. These results revealed the effects of Thermal annealing on the device morphology and its performance and efficiency.

INTRODUCTION

Organic solar cells (OSCs) evolved as a new solar cell technology and are in this respect very attractive as only very thin films of organic materials are needed, thus excluding the use of high energetic and cost intensive materials like silicon. Among OSCs different technologies have evolved − the most prominent ones are Dye-Sensitized, Bilayer, and Bulk Heterojunction Solar Cells. Due to their high technological interest, the development of OPV cells consisting of a polymer–fullerene bulk heterojunction (BHJ) has been rapid for the last few years. These nano scaled, flexible solar cells are an attractive new low cost green technology [1–3]. The polymer poly (3-hexylthiophene) (P3HT) blended with the fullerene derivative phenyl-C61-butyric acid methyl ester (PCBM), has been the most studied and successful system [4,5].

The Efficiency of these OPVs is highly depended on the fabrication of the appropriate morphology of this active blend [5–8]. Generally, the polymer and the fullerenes must be phase separated at 10–20 nm scale [8], providing thus large interfacial area for exciton dissociation. After charge separation the two phases must form pathways to the corresponding electrodes for efficient charge extraction. This ideal situation is difficult to be achieved in practice. For the optimization of morphology, different experimental methods have been proposed such as post thermal annealing [9–11], solvent annealing [12] or the use of additives [13,14] which can lead to rearrangement of the spin coated film by crystallization of both phases. However, upon annealing large phase separation with the formation of micrometer size PCBM crystals usually occurs. The growth mechanism of these crystals has been recently studied by several research groups [15–18]

For the study of the BHJs and to provide useful information about their morphology as well as the charge transport mechanisms have been done using Scanning Probe Microscopy techniques, such as Conductive AFM (C-AFM), Kelvin Probe Microscopy (KPM) [19–22], as well as Scanning near field Optical Microscope (SNOM) [16,23].

The effect of post thermal annealing on the nanoscale mechanical properties of large phase separated P3HT:PCBM BHJs have studied using Atomic Force Acoustic Microscopy (AFAM), Atomic Force Spectroscopy and Nanoindentation in correlation with their morphology and structure.

EXPERIMENTAL

In our study, we took a regioregular P3HT with an average molecular weight Mn = 45,000–65,000 and PCBM which were purchased from Aldrich. A solution of the blend P3HT:PCBM (1:0.8 w/w) was prepared in chlorobenzene with a total concentration of 18 mg/ml. The solution was stirred at for least 24 h and filtered prior to spin coating through a 0.45 μm syringe filter. Samples were prepared by spin coating (1000 rpm for 30 s) on microscope glass slides under nitrogen atmosphere in a glove box. First cleaned the Glass substrate with a detergent and then they were ultrasonicated in deionized water, acetone, isopropanol and methanol. After, they were dried on a hot plate and then were UV irradiated for 10 min.

For Annealing, the spin coated samples are then placed on a hot plate inside a glove box. For simplicity the Unannealed sample will be referred as Sample-RT and the Annealed samples as Sample-100 (100 °C) and Sample-145 (145 °C).

The Continuous Stiffness Measurements option of the NanoIndenter XP was used for the Nanoindentation (NI) testing, in order to study the nanomechanical properties of the P3HT:PCBM nanocomposites. The indents were made in several regions of the samples and specifically among the PCBM crystals in the case of the annealed samples, using a Berkovich diamond indenter. The hardness of the thin films is continuously measured versus the penetration depth using the following equation:

$$H = \frac{P}{A(h_c)} \qquad (1)$$

where P is the normal applied load and $A(h_c)$ is the contact area between the indenter and the sample. The h_c is the indentation contact depth estimated using the Oliver–Pharr method [24].

After this, AFAM was employed for the investigation of the near-surface mechanical properties of the P3HT:PCBM thin films. AFAM measurements were performed in contact mode, using rectangular silicon cantilevers with 10 nm nominal tip curvature.

The AFAM is a non destructive AFM technique, in which the AFM probe scans the sample's surface in contact mode and "records" the out-of-plane vibrations of the sample surface, which are caused by longitudinal acoustic waves emitted by a piezoelectric transducer, with 2.5 MHz central frequency. The transducer is placed below and in contact with the sample. This technique can provide sharp contrast variations of elasticity, while topography is simultaneously recorded in contact mode [25].

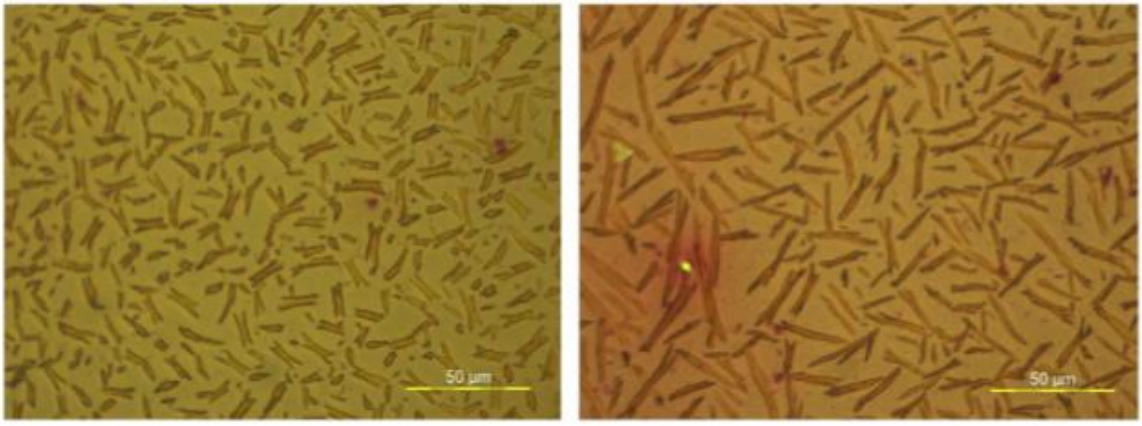

Fig. 1. Optical microscopy images of the P3HT:PCBM annealed: at 100 °C (left) and 145 °C (right) for 30 min.

Information about the structural characteristics of the P3HT:PCBM thin films was deduced by employing the X-ray diffraction (XRD) technique. The XRD measurements were performed at the 3–30° angular range, where the main reflections of the P3HT and the PCBM are apparent, with 0.04° step size and 0.5°/min scan speed.

RESULTS AND DISCUSSION

The results shows that, the Thermal Annealing of the P3HT:PCBM nanocomposites at 100 °C and 145 °C for 30 min caused the formation of large PCBM crystals, as it is shown in the optical microscopy images (Fig. 1). In sample-RT, these needle-like features (the PCBM crystals) are not visible. The size of the needle-like PCBM crystals is up to 20 µm and 50 µm, for T = 100 °C and T = 145 °C respectively, with random orientation [15–18]. In addition, smaller disc-like crystals are present, which possibly correspond to an earlier stage of the needle-like crystal growth. In areas where the density of the crystals is high, brush-like needles and pinholes are also observed.

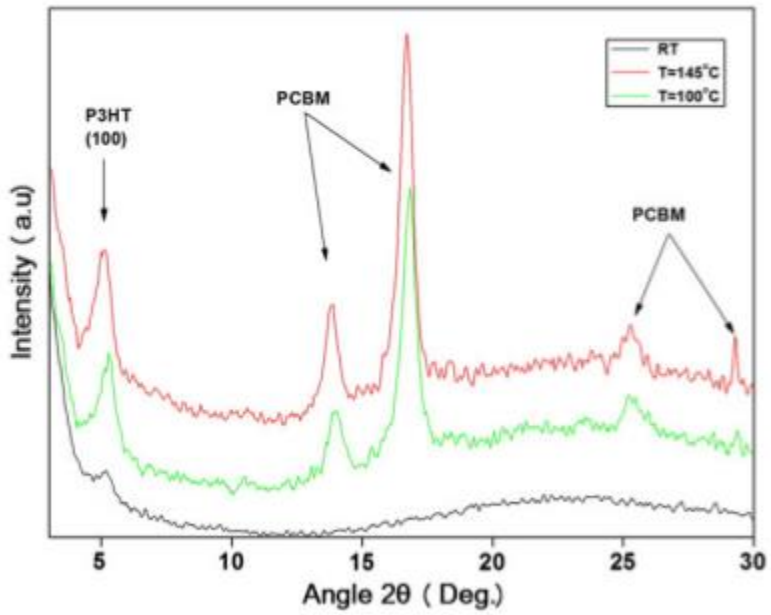

Fig. 2. XRD patterns of the P3HT:PCBM thin films before (RT) and after annealing at 100 °C and 145 °C for 30 min.

By using X-ray diffraction (XRD), the structural analysis of the samples was made and the Fig. 2 illustrates the effect of annealing on the structure of the P3HT:PCBM thin films. All the XRD profiles show a peak at 5.20° to 5.24°, which is associated with the (100) reflection of the P3HT. Specifically, this peak corresponds to a-axis orientation, with the main polymer chain parallel and the side chains perpendicular to substrate [26].

After annealing, the intensity of this peak increases, indicating an improvement of the degree of crystallinity. In addition, intense peaks at 13.9° and 16.7°, as well as less intense ones at 25.3° and 29.3°, associated with the PCBM, are observed. The foregoing peaks are the result of PCBM diffusion in the polymer matrix and the formation of large PCBM crystals, as shown in Fig. 1 [27]. The size of the P3HT crystallites was calculated using the (100) reflection and the Scherrer formula:

$$D_{hkl} = 0.9\lambda / \beta_{hkl}\cos\theta \qquad (2)$$

where D_{hkl} is the apparent crystallite size along the [*hkl*] direction and β_{hkl} is the full width at half maximum (FWHM) of an (*hkl*) diffraction (in radians). Statistical analysis of the peak profile reveals an increase of the FWHM (D_{100}) (0.47° to 0.55°) with the increase of the annealing temperature and as consequence, a decrease of the P3HT grain size.

Particularly, the P3HT crystallite size for sample-RT is 16.8 nm, whereas of the Annealed samples at 100 °C and 145 °C is 15.5 nm and 14.1 nm, respectively. The observed decrease of the P3HT

crystallite size is associated with the disordering of the polymer chains caused by the large PCBM clusters [28].

By setting the SPM probe (cantilever) in contact with the sample surface, the so-called acoustic images can be acquired, which represent the vibration amplitude of the cantilever. The effect of annealing on the local near-surface nanomechanical properties was studied using AFAM. AFAM enables the mapping of the surface mechanical properties so that the surface regions with different mechanical responses can be distinguished. In Fig. 3 the topography and the corresponding AFAM image of the P3HT:PCBM thin film annealed at 100 °C are presented. A typical PCBM needle-like crystal with 20 μm length and 300 nm height can be seen. Disc-like crystals are also observed in the upright corner of the image.

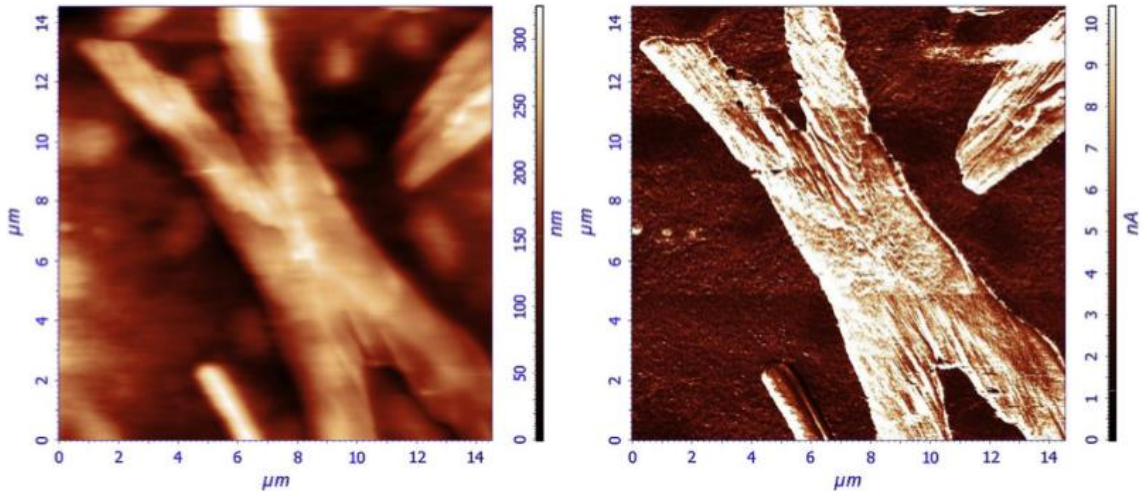

Fig. 3. AFM topography (contact mode) and the corresponding AFAM image. Scan size is 14.5 × 14.5 μm2.

In the topography image, the dark regions that surround the PCBM crystal indicate the large height deviation between the PCBM crystal and the polymer, which occurred by the PCBM molecules diffusion into the growing crystal and resulted to the local decrease of the thin film thickness [29]. In the AFAM image, the lighter surface regions correspond to material with greater stiffness. The PCBM crystals show sharp contrast comparing to the surrounding regions. While this was expected, the more interesting is that the P3HT aggregates, which are close to the PCBM crystals, appear to be darker compared to the rest of the P3HT. Thus, these aggregates are consisted of amorphous P3HT.

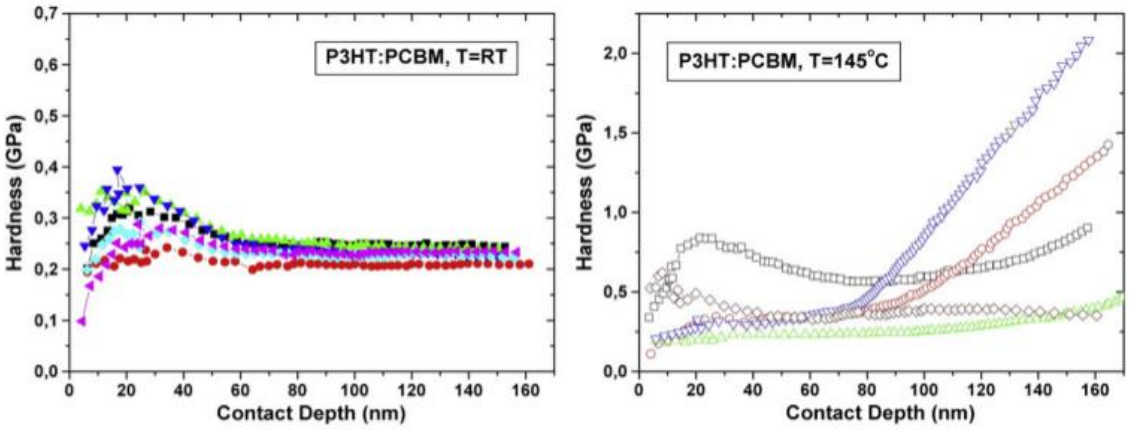

Fig. 4. The hardness of the P3HT:PCBM, before (left) and after the annealing at 145 °C (right), versus the nanoindentation contact depth.

In Fig. 4 the NI hardness (H) of the P3HT:PCBM/glass samples, before (left) and after (right) annealing at 145 °C, versus the contact depth (hc) is presented.

In the case of the sample-RT, the H values for hc =0–40 nm appear to be higher than those of the value plateau (H ≈ 0.25 GPa) for hc N 40 nm. This happens due to: i) the NI inherent limitations. The A(hc) does not accurately describe the indenter geometry for very swallow depths and as a consequence the H is overestimated and ii) the nanocomposite organic material mechanical properties, which are generally time-depended. It should also be noted that the nanomechanical behavior of the sample-RT is uniform, because the H values at the plateau region are almost the same no matter the surface location of the indent.

In contrast, the H values of the annealed P3HT:PCBM coming from different indents present a variation that corresponds to an inhomogeneous material. The indents to this sample were made in regions between the PCBM crystals. Also, an abrupt increase of the H values after a certain hc is observed. This happens due to the so-called substrate effect [30]. The substrate effect at the different surface locations starts at different hc due to the inhomogeneous P3HT:PCBM thickness, which is occurred after the annealing.

Atomic Force Spectroscopy has been successfully used for the investigation of the local mechanical properties of soft, polymeric and biological materials [31]. In this work, stiff (k= 12–22.5 N/m), rectangular Si cantilevers and applied forces up to few μN were used to study the local mechanical properties of the P3HT:PCBM. It should be noted that: i) the cantilevers' tips are coated with 70 nm thick diamond coating and ii) the nominal radius of the tip curvature is 70 nm. The spring constant of each cantilever was measured by the normal Sader method [32], which is reliable for rectangular cantilevers.

Before AFS the samples were scanned in AFM semi-contact mode, in order to locate the appropriate surface regions. Then, for the AFS, switching to contact mode was made and a

calibration of the optical system sensitivity was performed. The vertical deflection DFL (nA) signal was recorded and converted to force by taking into account the cantilever's k and the Hooke's law. So, the corresponding Force (nN)–Piezo Displacement (nm) (F–D) curves were produced for each AFS at various locations on the sample's surface.

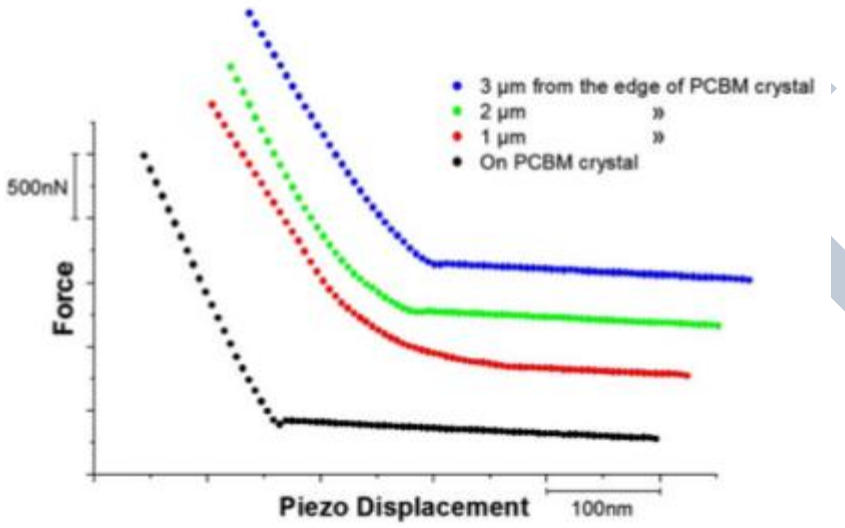

Fig.5. Representative Force (nN)–Piezo Displacement (nm) curves on PCBM crystal and in various distances from the edge of the PCBM crystal.

Over 100 curves at various applied loads were obtained at different sample areas of interest. Fig. 5 shows representative force–distance curves for the annealed Sample-100. The F–D curves are from the PCBM crystal and from regions at various distances from the PCBM edge (1–3 μm). The maximum applied force is 2 μN. On the right part of the curve (parallel to X-axis), the probe is approaching the surface and interact with the material via long range repulsive force. When the probe is close to the surface, the attractive Van der Waals and capillary forces cause a jump-in to contact with the sample's surface. This 'snap in to contact' point is easily defined on hard surfaces, like this of the PCBM crystal. From this contact point, the tip starts to apply force on the surface and the curve slope can provide information about the nanomechanical properties of the sample.

Thus, from the F–D curves the PCBM appears to be stiffer than the surrounding P3HT material, in accordance with the AFAM results. The F–D curves show a progressive increase of the surface stiffness with the increase of the distance from the PCBM crystal edge. This means that the areas close to the PCBM crystals are P3HT-rich or PCBM-depleted [16,18].

Concerning the required force, which should be applied in order to plastically deform the several areas of the annealed P3HT:PCBM samples, it was found that:

i) For F ≤ 1 μN only the P3HT aggregates, which are close to the PCBM crystals, were plastically deformed.

ii) For F ≥ 4 μN (Fig. 6) the sample-RT was plastically deformed. For F = 4 μN, the indent impression was ~ 30 nm deep.

iii) For F ≈ 18 μN the annealed Sample-100 was plastically deformed and the indent impression was 28 nm deep.

iv) The maximum force that can be applied by this type of Si cantilevers is Fmax ≈ 18 μN and it was not possible to plastically deform the PCBM crystals with such low applied force.

In Fig. 6, the previously described residual impressions of the indents are presented.

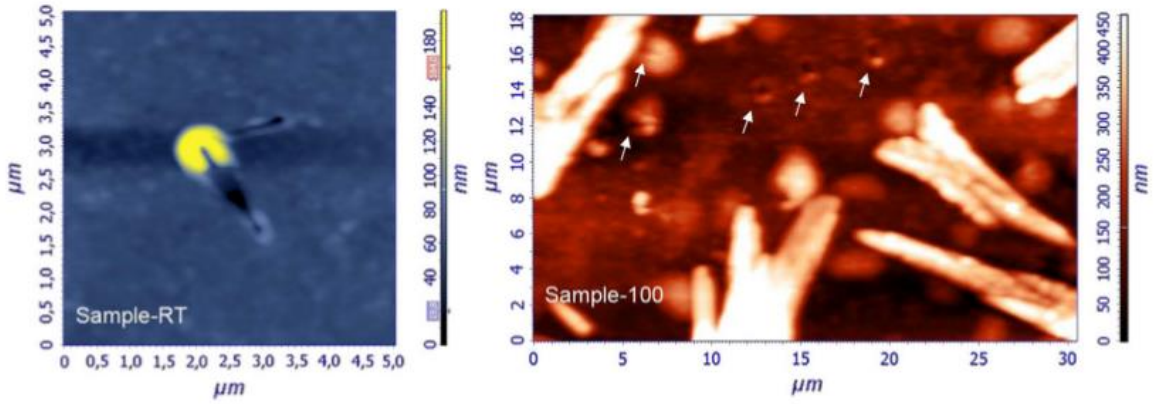

Fig. 6. AFM images showing the residual impression of the indents made on the surface of the P3HT:PCBM samples by AFS.

CONCLUSIONS

The morphological effect of thermal annealing on the device structure and the surface distribution of the several structural features formed after annealing was studied in the light of their nanomechanical response. By increasing the thermal annealing temperature, it causes an increasing of the size of the PCBM crystallites and to the crystallinity of the two phases (PCBM and P3HT). In addition to the capability of measuring with nanometer precision the local mechanical properties of BHJs by AFM Force Spectroscopy, in both elastic and plastic regimes, enabled the discrimination of the several structural features of the P3HT and their mapping/distribution in relation to their distance from the PCBM crystallites. Polyalkylthiophene/fullerene nanocomposites are the most promising materials for application in organic photovoltaic devices. Their efficiency is directly connected to the structure and phase separation, while the nanocomposite mechanical properties affect the device service life.

REFERENCES

[1] S. Logothetidis, Mater. Sci. Eng., B 152 (2008) 96.
[2] A.C. Mayer, S.R. Scully, B.E. Hardin, M.W. Rowell, M.D. McGehee, Mater. Today 10 (2007) 28.
[3] M.-C. Choi, Y. Kim, C.-S. Ha, Prog. Polym. Sci. 33 (2008) 581.
[4] P.A. Troshin, H. Hoppe, J. Renz, M. Egginger, J.Yu. Mayorova, A.E. Goryachev, A.S. Peregudov, R.N. Lyubovskaya, G. Gobsch, N.S. Sariciftci, V.F. Razumov, Adv. Funct. Mater. 19 (2009) 779.
[5] H. Hoppe, N.S. Sariciftci, J. Mater. Chem. 16 (2006) 45.
[6] S.S. van Bavel, E. Sourty, G. de With, J. Loos, Nano Lett. 9 (2009) 507.
[7] K. Maturova, S.S. van Bavel, M.M. Wienk, R.A.J. Janssen, M. Kemerink, Nano Lett. 9 (2009) 3032.
[8] Wanli Ma, Cuiying Yang, Alan J. Heeger, Adv. Mater. 19 (2007) 1387. 4109
[9] F. Padinger, R.S. Rittberger, N.S. Sariciftci, Adv. Funct. Mater. 13 (2003) 85.
[10] W. Ma, C. Yang, X. Gong, K. Lee, A.J. Heeger, Adv. Funct. Mater. 15 (2005) 1617.
[11] G. Li, Y. Yao, H. Yang, V. Shrotriya, G. Yang, Y. Yang, Adv. Funct. Mater. 17 (2007) 1636.
[12] J.K. Lee, Wan L. Ma, C.J. Brabec, J. Yuen, J.S. Moon, J.Y. Kim, K. Lee, G.C. Bazan, A.J. Heeger, J. Am. Chem. Soc. 130 (2008) 3619.
[13] L.-M. Chen, Z. Hong, G. Li, Y. Yang, Adv. Mater. 21 (2009) 1434.
[14] A. Swinnen, I. Haeldermans, M. vande Ven, J. D'Haen, G. Vanhoyland, S. Aresu, M. D'Olieslaeger, J. Manca, Adv. Funct. Mater. 16 (2006) 760.
[15] E. Klimov, W. Li, X. Yang, G.G. Hoffmann, J. Loos, Macromolecules 39 (2006) 4493.
[16] J. Jo, S.-S. Kim, S.-I. Na, B.-K. Yu, D.-Y. Kim, Adv. Funct. Mater. 19 (2009) 866.
[17] B. Watts, W.J. Belcher, L. Thomsen, H. Ade, P.C. Dastoor, Macromolecules 42 (2009) 8392.
[18] L.S.C. Pingree, O.G. Reid, D.S. Ginger, Adv. Mater. 21 (2009) 19.
[19] O. Douhéret, L. Lutsen, A. Swinnen, M. Breselge, K. Vandewal, L. Goris, J. Manca, Appl. Phys. Lett. 89 (2006) 032107.
[20] Y.-C. Huang, S.-Y. Chuang, M.-C. Wu, H.-L. Chen, C.-W. Chen, W.-F. Su, J. Appl. Phys. 106 (2009) 034506.
[21] H. Hoppe, T. Glatzel, M. Niggemann, A. Hinsch, M.Ch. Lux-Steiner, N.S. Sariciftci, Nano Lett. 5 (2) (2005) 269.
[22] M.-C. Wu, H.-H. Lo, H.-C. Liao, S. Chen, Y.-Y. Lin, W.-C. Yen, T.-W. Zeng, Y.-F. Chen, C.-W. Chen, W.-F. Su, Sol. Energy Mater. Sol. Cells 93 (2009) 869.
[23] W.C. Oliver, G.M. Pharr, J. Mater. Res. 7 (1992) 1564.
[24] NT-MDT, Atomic Force Acoustic Microscopy – Instruction Manual.
[25] T. Erb, S. Raleva, U. Zhokhavets, G. Gobsch, B. Stühn, M. Spode, O. Ambacher, Thin Solid Films 450 (2004) 97.
[26] D. Chirvase, J. Parisi, J.C. Hummelen, V. Dyakonov, Nanotechnology 15 (2004) 1317.
[27] M.-Y. Chiu, U.-S. Jeng, C.-H. Su, K.S. Liang, K.H. Wei, Adv. Mater. 20 (2008) 2573.
[28] H. Zhong, X. Yang, B. de With, J. Loos, Macromolecules 39 (2006) 218.

[29] S. Logothetidis, S. Kassavetis, C. Charitidis, Y. Panayiotatos, A. Laskarakis, Carbon 42 (2004) 1133.
[30] B. Cappella, G. Dietler, Surf. Sci. Rep. 34 (1999) 1.
[31] J.E. Sader, J.W.M. Chon, Rev. Sci. Instrum. 70 (10) (1999) 3967.
[32] M. C. Scharber, D. Mühlbacher, M. Koppe, P. Denk, C. Waldauf, A. J. Heeger, C. J. Brabec, *Adv. Mater.* 2006, *18*, 789.